


Effects of frequency-dependent Kerr nonlinearity on higher-order soliton evolution in a photonic crystal fiber with one zero-dispersion wavelength

Saili Zhao ^{1,2,*}, Ruijun Guo,¹ and Yong Zeng ¹

¹Henan Key Laboratory of Laser and Opto-Electric Information Technology, School of Electric and Information Engineering, Zhengzhou University, Zhengzhou 450001, China

²Institute of Intelligent Sensing, Zhengzhou University, Zhengzhou 450001, China

 (Received 21 April 2022; revised 16 August 2022; accepted 9 September 2022; published 23 September 2022)

We show that the higher-order soliton evolution can be considerably affected by the relative positions of the zero-nonlinearity wavelength (ZNW) and zero-dispersion wavelength (ZDW) with respect to the input wavelength in photonic crystal fibers (PCFs) with frequency-dependent Kerr nonlinearity. By regulating the magnitude of nonlinear dispersion, the position of the ZNW and the strength of the doping Kerr nonlinearity can vary to a large extent, which significantly changes the general process of higher-order soliton evolution in the PCFs. Particularly, some interesting phenomena observed numerically in the PCFs with one ZDW and one ZNW are as follows: the formation of a blueshifted fundamental soliton that satisfies the phase-matching and group-velocity-matching conditions with a redshifted fundamental soliton, the tunneling effect of a fundamental soliton that transfers from one solitonic region to another one through a spectrally limited nonsolitonic region, and the generation of the high-intensity blueshifted dispersive wave and redshifted dispersive wave.

DOI: [10.1103/PhysRevA.106.033516](https://doi.org/10.1103/PhysRevA.106.033516)

I. INTRODUCTION

Considerable effort has been devoted to the investigation of the evolution of higher-order solitons due to their fundamental impact on nonlinear wave propagation as well as some exciting applications such as supercontinuum light sources and soliton lasers [1–3]. Since photonic crystal fibers (PCFs) have some unique optical properties such as high nonlinearity, low confinement loss, and tunable chromatic dispersion, they are widely used as powerful research platforms for higher-order soliton evolution [4,5]. In the conventional PCFs with positive nonlinearity covering all wavelengths, the zero-dispersion wavelength (ZDW) separates a solitonic region with anomalous dispersion from a nonsolitonic one with normal dispersion. In the PCFs with one ZDW, the longer wavelength edge of the generated spectrum is controlled by redshifted fundamental solitons ejected via soliton fission while the shorter wavelength edge is dominated by blueshifted dispersion waves (BDWs) radiated via satisfying the phase-matching condition [2]. In the PCFs with two ZDWs, the generated spectrum is bounded by two branches of dispersive waves (DWs), namely, BDWs and redshifted dispersive waves (RDWs) [6,7]. However, the Raman-induced frequency shift of the fundamental soliton is suppressed in the vicinity of the second ZDW due to the process of spectral recoiling associated with RDWs. In the PCFs with three ZDWs, an attractive phenomenon known as the soliton spectral tunneling (SST) effect is given rise by a Raman-induced soliton self-frequency shift. In this case, the energy of the fundamental soliton is continuously shed off from one anomalous dispersion region to another after passing through a narrow normal-dispersion

region sandwiched in between [8–11]. Such rich phenomena of soliton dynamics exhibited in the PCFs with one or multiple ZDWs mainly result from the flexibly tunable dispersion characteristics together with the positive nonlinear properties.

Recently, increasing attention has gradually been paid to higher-order soliton evolution in the PCFs with frequency-dependent Kerr nonlinearity, which is achieved by doping the core glass with metal nanoparticles [12–16]. Unlike the traditional PCFs with positive nonlinearity at all wavelengths, the doped PCFs offer additional control over the Kerr nonlinearity that can vary considerably with wavelength and even changes its numeric sign from positive to negative across a zero-nonlinearity wavelength (ZNW) [17–20]. Here the ZNW is a specific wavelength at which the optical Kerr nonlinearity vanishes. In particular, the coexistence of ZNW and ZDW makes it possible to achieve multiple spectral regions with different signs of the dispersion and nonlinear coefficients, which plays a significant role in manipulating the formation and distribution of the fundamental solitons and DWs [17–19]. For example, the existence of negative nonlinearity allows the fundamental solitons formed even in the normal-dispersion region, which is not common in conventional fibers. Since the change in frequency dependence of doping Kerr nonlinearity can dramatically regulate the position of ZNW and the nonlinear strength acting on the spectral components, it is very meaningful to explore the combination action of ZDW and ZNW on the effect of higher-order soliton evolution. By altering the frequency dependence of doping nonlinearity, some phenomena of soliton dynamics common in the PCFs with multiple ZDWs can also be exhibited in the PCFs with one ZDW and one ZNW.

In this paper, we numerically study the higher-order soliton evolution in the PCFs exhibiting one ZNW in addition to one ZDW. Numerical results show that the soliton dynamics can

*iesallyzhao@zzu.edu.cn

be considerably affected by the relative positions of the ZNW and ZDW with respect to the input wavelength. Note that all soliton dynamics discussed here occur in a single spatial core mode. This paper is organized as follows. In Sec. II, we introduce the propagation model for studying higher-order soliton evolution in the PCFs with frequency-dependent Kerr nonlinearity. Moreover, a stable dispersion property as well as the varying doping nonlinearity including different nonlinear dispersion coefficients are presented in this section. In Sec. III, we show that regulating the magnitude of the doping Kerr nonlinearity and the interval between ZNW and ZDW can stimulate different phenomena of soliton dynamics during the higher-order soliton evolution. The main conclusions are summarized in Sec. IV.

II. NUMERICAL MODEL AND FIBER PROPERTIES

The evolution of the higher-order soliton pulse in the PCFs with frequency-dependent Kerr nonlinearity can be modeled by a well-modified generalized nonlinear Schrödinger equation (GNLSE) [1,18]. Note that the metal nanoparticles for adjusting the Kerr nonlinearity have no effect on Raman contribution. Hence, the Raman-induced spectral blueshift that appears to be nonphysical can be avoided during the pulse evolution [18–20]. Based on the above assumption, the adopted GNLSE is formulated in terms of the electric-field envelope $A = A(z, t)$, which is at a propagation distance z in a retarded reference time frame $t = \tau - z/v_g = \tau - \beta_1 z$ traveling at the envelope group velocity $v_g = 1/\beta_1$, taking the following form:

$$\frac{\partial A}{\partial z} - \sum_{n \geq 2} \frac{i^{n+1} \beta_n}{n!} \frac{\partial^n A}{\partial t^n} = i(1 - f_R) \gamma_{\text{eff}} |A(z, t)|^2 A(z, t) + i f_R \gamma A(z, t) \int_0^\infty h_R(t') |A(z, t - t')|^2 dt'. \quad (1)$$

The left-hand side of Eq. (1) models linear propagation effects with β_n as the n th-order dispersion coefficients. The right-hand side models nonlinear effects with γ and γ_{eff} as frequency-dependent nonlinear coefficients of the undoped and doped regions, respectively. $\gamma(\omega) \approx \gamma_0 + \gamma_1(\omega - \omega_0)$ and $\gamma_{\text{eff}}(\omega)$ are defined as [19]

$$\begin{aligned} \gamma_0 &= \frac{2\pi n_2}{\lambda_0 A_{\text{eff}}}, & \gamma_1 &\approx \frac{\gamma_0}{\omega_0}, & \gamma_{\text{eff}} &= \frac{2\pi \text{Re}(n_{2\text{eff}})}{\lambda_0 A_{\text{eff}}}, \\ n_2 &= \frac{3\chi_h^{(3)}}{4\epsilon_0 c}, & n_{2\text{eff}} &= \frac{3\chi_{\text{eff}}^{(3)}}{4\epsilon_0 c \epsilon_{\text{eff}}}, \\ \epsilon_{\text{eff}} &= \frac{\epsilon_h(1 + 2f\sigma)}{1 - f\sigma}, & \sigma &= \frac{\epsilon_i - \epsilon_h}{\epsilon_i + 2\epsilon_h}. \end{aligned}$$

The core glass of PCFs used in this paper is made of silver nanoparticle-doped silica glass. Thus ϵ_i and ϵ_h are the dielectric functions of silver and silica, respectively. The filling factor f is the volume fraction of the silver nanometric inclusions. $\chi_{\text{eff}}^{(3)}$ is the effective third-order susceptibility in the presence of silver nanoparticles, and $\chi_h^{(3)}$ is the third-order

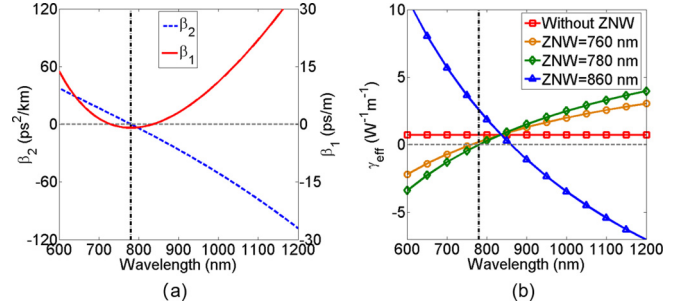


FIG. 1. (a) At the pump wavelength of 835 nm, the group-velocity dispersion (β_2) curve and relative group-delay (β_1) curve of the PCF as a function of wavelength. (b) The effective doping nonlinear coefficient γ_{eff} as a function of wavelength for $\gamma_{1\text{eff}} = 0$ (red curve with square, without ZNW), $\gamma_{1\text{eff}} = -3.3456 \times 10^{-3} \text{ W}^{-1} \text{ m}^{-1} \text{ ps}$ (orange curve with circle, ZNW = 760 nm), $\gamma_{1\text{eff}} = -4.6822 \times 10^{-3} \text{ W}^{-1} \text{ m}^{-1} \text{ ps}$ (green curve with rhombus, ZNW = 780 nm), $\gamma_{1\text{eff}} = 1.1357 \times 10^{-2} \text{ W}^{-1} \text{ m}^{-1} \text{ ps}$ (blue curve with triangle, ZNW = 860 nm). The vertical dot-dashed black lines in (a), (b) mark the ZDW located at 780 nm.

susceptibility of the host glass. $\chi_{\text{eff}}^{(3)}$ can be calculated using a theory of composite nonlinear materials as follows [19]:

$$\chi_{\text{eff}}^{(3)} = f \frac{\chi_i}{|B|^2 B^2} + \chi_h \frac{D}{|1 - f\sigma|^2 (1 - f\sigma)^2}, \quad (2)$$

$$B = \frac{(1 - f\sigma)(\epsilon_i + 2\epsilon_h)}{3\epsilon_h}, \quad (3)$$

$$D = 1 - f\{1 - 0.4(4\sigma^2|\sigma|^2 + 4\sigma|\sigma|^2 + \sigma^3 + 9|\sigma|^2 + 9\sigma^2)\}. \quad (4)$$

The susceptibilities of host silica glass and silver are $\chi_h = 2.233 \times 10^{-22} \text{ m}^2/\text{V}^2$ and $\chi_i = (-6.3 + i1.9) \times 10^{-16} \text{ m}^2/\text{V}^2$, respectively. Since the volume fraction of silver nanoparticles in the doped region is small, the Raman response function of the doped PCF is considered to be the same as the general silica PCFs [17–19]. Thus in Eq. (1), the Raman fraction is $f_R = 0.18$ and the Raman response function is $h_R(\tau) = \exp(-\tau/\tau_2) \sin(-\tau/\tau_1) (\tau_1^2 + \tau_2^2) / \tau_1 \tau_2^2$ with the Raman period $\tau_1 = 12.2 \text{ fs}$ and lifetime $\tau_2 = 32 \text{ fs}$.

In this paper, a hyperbolic secant pulse at a center wavelength of 835 nm with 50 fs pulse width is used as the pump source. A 1.2-m-long PCF with single ZDW located at 780 nm serves as the propagation medium [1,2]. At the pump wavelength of 835 nm, the group-velocity dispersion (β_2) curve and relative group delay (β_1) curve of the PCF as a function of the wavelength are shown in Fig. 1(a), whose dispersion coefficients are up to tenth order, as follows: $\beta_2 = -11.830 \text{ ps}^2/\text{km}$, $\beta_3 = 8.1032 \times 10^{-2} \text{ ps}^3/\text{km}$, $\beta_4 = -9.5205 \times 10^{-5} \text{ ps}^4/\text{km}$, $\beta_5 = 2.0737 \times 10^{-7} \text{ ps}^5/\text{km}$, $\beta_6 = -5.3943 \times 10^{-10} \text{ ps}^6/\text{km}$, $\beta_7 = 1.3486 \times 10^{-12} \text{ ps}^7/\text{km}$, $\beta_8 = -2.5495 \times 10^{-15} \text{ ps}^8/\text{km}$, $\beta_9 = 3.0524 \times 10^{-18} \text{ ps}^9/\text{km}$, and $\beta_{10} = -1.7140 \times 10^{-21} \text{ ps}^{10}/\text{km}$. The nonlinear coefficients of the undoped region at 835 nm are $\gamma_0 = 0.11 \text{ W}^{-1} \text{ m}^{-1}$ and $\gamma_1 \approx \gamma_0/\omega_0 \approx 4.8728 \times 10^{-5} \text{ W}^{-1} \text{ m}^{-1} \text{ ps}$. The silica core of the PCF doped with silver nanoparticles exhibits a Kerr nonlinearity γ_{eff} varying significantly with wavelength and even changing the

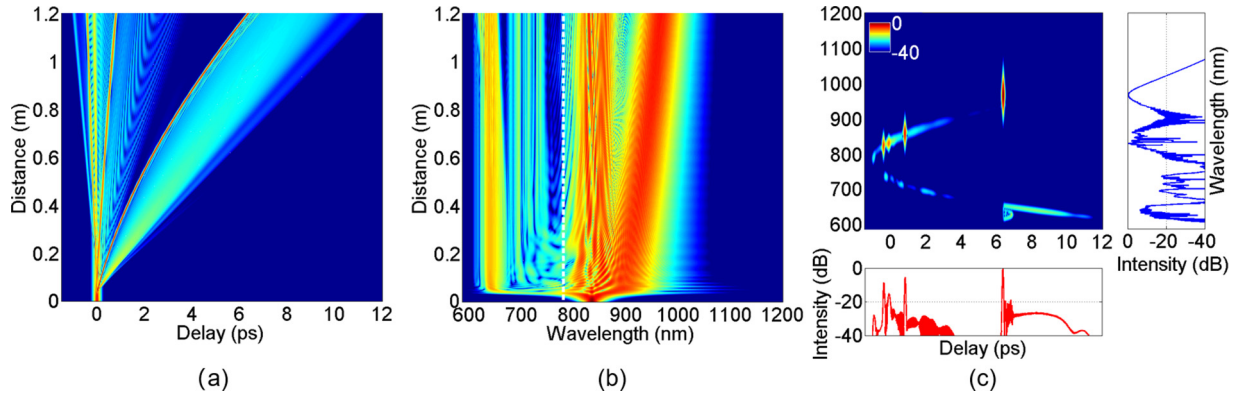


FIG. 2. (a) Temporal and (b) spectral evolutions of higher-order soliton in a 1.2-m-long PCF with only one ZDW but no ZNW for $\gamma_{1\text{eff}} = 0$. (c) The corresponding spectrogram as well as the temporal and spectral profiles at the PCF output. The vertical white dashed line in (b) marks the ZDW at 780 nm.

sign at the ZNW [19–21]. Namely, $\gamma_{\text{eff}} > 0$ indicates positive nonlinearity and $\gamma_{\text{eff}} < 0$ indicates negative nonlinearity. The Taylor series expansion of γ_{eff} around the operating frequency provides the higher-order terms of the Kerr nonlinear coefficient. Thus the frequency dependence of γ_{eff} can be taken into account using $\gamma_{\text{eff}}(\omega) = \gamma_{0\text{eff}}(\omega_0) + \gamma_{1\text{eff}}(\omega - \omega_0)$, where $\gamma_{0\text{eff}} = 0.7453 \text{ W}^{-1} \text{ m}^{-1}$ and $\gamma_{1\text{eff}} = d\gamma_{\text{eff}}/d\omega$ is evaluated at the pump frequency ω_0 for the volume fraction of silver nanoparticle inclusions. In order to study how the frequency-dependent Kerr nonlinearity affects the higher-order soliton evolution in the PCF with one ZDW, the input pulse with peak power $P_0 = 159 \text{ W}$ is chosen to excite the soliton order $N = T_0 \sqrt{|\gamma_{0\text{eff}}| P_0 / |\beta_2|} \approx 5$ at the input end of the PCF [18,19]. Figure 1(b) shows the effective doping nonlinear profiles γ_{eff} as a function of the wavelength at the different nonlinear dispersion coefficients $\gamma_{1\text{eff}}$ for the PCF. It can be clearly observed that the value and numeric sign of $\gamma_{1\text{eff}}$ control the position of the ZNW and the slope of the effective doping nonlinearity.

III. NUMERICAL SIMULATIONS FOR HIGHER-ORDER SOLITON EVOLUTION IN PCFs

Figure 2 shows the evolution of a higher-order soliton in a PCF with only one ZDW but no ZNW, which is achieved by setting $\gamma_{1\text{eff}} = 0$. In this case, the positive Kerr nonlinearity covers the PCF at all wavelengths. Since the solitonic region corresponds to a wavelength range in which β_2 and γ_{eff} have opposite signs, the ZDW at 780 nm separates a solitonic region from a nonsolitonic one. In the initial stage of spectral evolution, self-phase modulation (SPM) broadens the spectrum by generating new frequency components. Accordingly, strong temporal compression occurs over this range. When the spectrum is broadened to the greatest degree by SPM, a series of fundamental solitons is ejected into the solitonic region by balancing the interaction between anomalous group-velocity dispersion and the SPM induced by positive Kerr nonlinearity. Then the associated BDWs are radiated into the nonsolitonic region from these ejected fundamental solitons via satisfying the phase-matching condition under the effect of higher-order dispersion. Even though the redshifted Raman solitons and BDWs have separated optical spectra, they can overlap in the time domain, as shown in Fig. 2(c). The BDWs in the nonsoli-

tonic region can be trapped by the potential barrier presented by the decelerating soliton in the solitonic region, leading to the formation of a trapping DW. Here the trapping effect of the DW by the soliton is triggered by the group-velocity matching between the soliton and the DW, which critically depends on the walk-off dynamics between the two components [7,22].

When $\gamma_{1\text{eff}} = -4.6822 \times 10^{-3} \text{ W}^{-1} \text{ m}^{-1} \text{ ps}$, solitons can be supported in all parts of the spectrum except at 780 nm because of the coincidence between ZNW and ZDW. In this case, the interplay between negative nonlinearity and normal dispersion can lead to an interesting dynamic where blueshifted Raman solitons can be generated along with the phase-matched radiation. As shown in Fig. 3, the input higher-order soliton pulse breaks up into a series of redshifted fundamental solitons and the associated blueshifted fundamental soliton through soliton fission under the combined action of Kerr nonlinearity and dispersion effect. Since the group-velocity-matching condition is satisfied between the first-generated redshifted soliton (labeled by ①) and the first-generated blueshifted one (labeled by ④), the two solitons overlap in the time domain while they separate in the spectral domain, as shown in Fig. 3(d). The outcome of such solitonic interactions also depends on the relative phases of the solitons. Additionally, another two fundamental solitons labeled by ② and ③ in Fig. 3(d) are ejected in the anomalous dispersion region. Since the two fundamental solitons (② and ③) initially have a little negative time delay shown in Fig. 3(a), they are ejected between the ZDW and pump wavelength. It is well known that the soliton ejected earlier has higher amplitude, shorter pulse width and faster group velocity [1,2]. Thus, in order to keep the form of the standard fundamental soliton, the first-ejected one (②) of the two soliton (② and ③) needs to be formed at a shorter wavelength. Subsequently, the fundamental soliton (②) first accelerates a little, then slows down quickly, and finally collides with another soliton (③) under the combined action of group-velocity dispersion and Raman effect, as shown in Fig. 3(a). During the soliton collision, energy transfer and velocity change happen to the two solitons (② and ③) following the conservation of momentum and energy, which results in the fundamental soliton with higher power gaining some energy from the other soliton and having a larger redshifted velocity [23]. The phenomena of soliton collision and energy transfer can also be clearly observed in

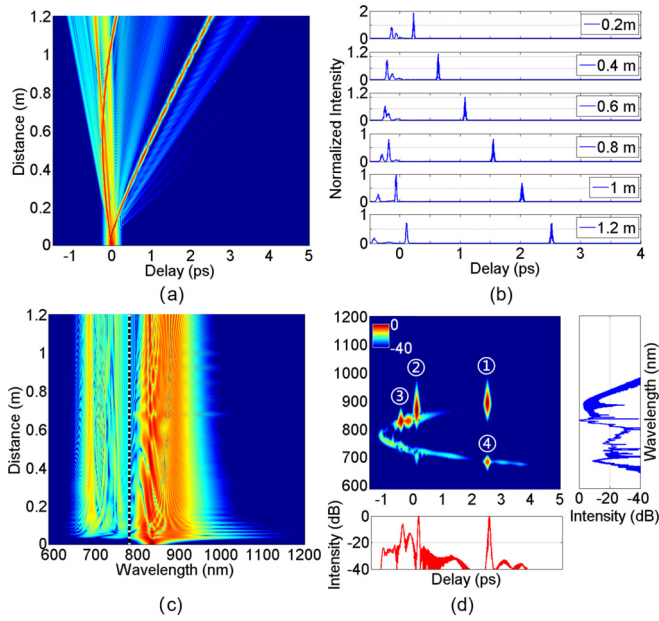


FIG. 3. (a) Temporal and (c) spectral evolutions of higher-order soliton in a 1.2-m-long PCF with one ZNW located at 780 nm for $\gamma_{\text{eff}} = -4.6822 \times 10^{-3} \text{ W}^{-1} \text{ m}^{-1} \text{ ps}$. (b) The corresponding pulse shapes at different propagation distances. (d) The corresponding spectrogram as well as the temporal and spectral profiles at the PCF output. The vertical white (black) dashed line in (c) marks the ZDW (ZNW) at 780 nm. The serial number in (d) marks the generated fundamental solitons.

Fig. 3(b). Then the fundamental soliton (②) continues to redshift toward the longer wavelength at a gradually increasing velocity because of the Raman effect. Meanwhile, the soliton (②) transfers some energy to a narrow-band resonance in the normal-dispersion region in the presence of higher-order dispersion, as shown in Fig. 3(d). Note that the phase-matching and group-velocity-matching conditions are satisfied between the narrow-band resonance and the redshifted fundamental soliton. When the blueshifted narrow-band resonance gains enough energy from the corresponding redshifted fundamental soliton, it can also be converted into a fundamental soliton in the normal-dispersion solitonic region.

When γ_{eff} increases to $-3.3456 \times 10^{-3} \text{ W}^{-1} \text{ m}^{-1} \text{ ps}$, the ZNW is located at 760 nm and has a 20-nm gap with the ZDW. In this PCF, these wavelengths between 760 and 780 nm belong to the nonsolitonic region while those shorter than 760 nm or longer than 780 nm become the solitonic regions. The existence of multiple solitonic regions with a minor interval provides a basic prerequisite for the occurrence of the SST phenomenon. Previous studies on SST mainly focused on the fibers with multiple ZDWs, which enables a soliton to tunnel from one anomalous dispersion region to another one through a spectrally limited regime of normal dispersion [8–11]. Here we show how one soliton can tunnel from one solitonic region to another one through a narrow nonsolitonic region in the PCF with one ZDW and one ZNW.

In the initial stage of propagation, the SPM causes the input higher-order soliton pulse to be compressed in the time domain and broadened in the spectral domain. Subsequently, higher-order dispersion and Raman scattering become the two

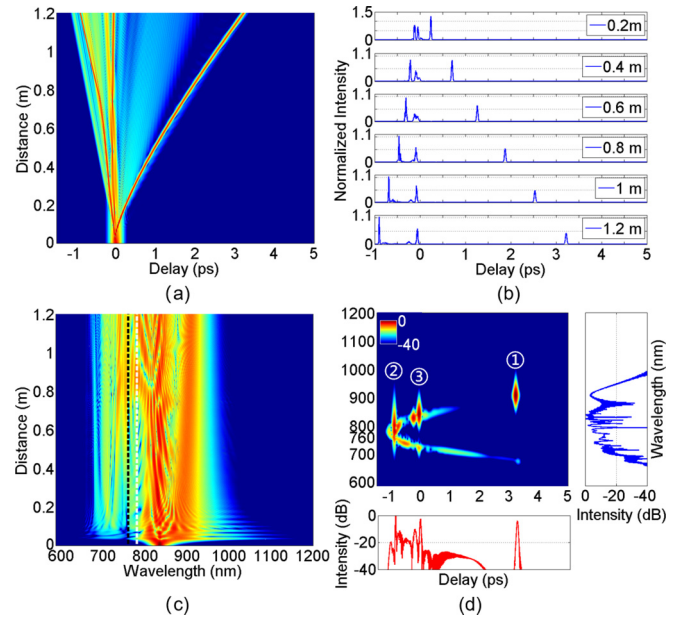


FIG. 4. (a) Temporal and (c) spectral evolutions of higher-order soliton in a 1.2-m-long PCF with one ZNW located at 760 nm for $\gamma_{\text{eff}} = -3.3456 \times 10^{-3} \text{ W}^{-1} \text{ m}^{-1} \text{ ps}$. (b) The corresponding pulse shapes at different propagation distances. (d) The corresponding spectrogram as well as the temporal and spectral profiles at the PCF output. The vertical white (black) dashed line in (b) marks the ZDW (ZNW) at 780 nm (760 nm). The serial number in (d) marks the generated fundamental solitons.

most significant effects, which break up the pulse into a series of fundamental solitons through soliton fission and the emission of nonsolitonic radiation via satisfying the phase-matching condition. It is well known that the earlier the fundamental soliton is ejected, the higher its peak power and the narrower the temporal width. As shown in Figs. 4(a) and 4(c), the first-ejected fundamental soliton (labeled by ①) is formed at the longest wavelength in contrast with the subsequently ejected ones (labeled by ② and ③) and then continues to redshift under the Raman effect. As the first-ejected fundamental soliton gradually redshifts toward the longer wavelength and undergoes an increasing nonlinear strength, it constantly radiates some energy into another solitonic region to form the phase-matched DW. Thus the first-ejected fundamental soliton has a decreasing peak intensity and an increasing temporal width along with the propagation distance, as shown in Fig. 4(b). Under the combined action of dispersion effect and Kerr nonlinearity, the second-ejected fundamental soliton (labeled by ②) generated between the ZDW and the pump wavelength begins to blueshift. As the soliton (②) blueshifts toward the shorter wavelength, it needs to constantly compress its pulse width and increase its peak power to ensure that $N = 1$ since the γ_{eff} it undergoes gradually decreases. Moreover, the soliton (②) also transfers some energy to the DWs that, as soliton-induced optical Cherenkov radiation, are resonant waves meeting the phase-matching condition with the soliton. Although the DW has a fairly high energy, it is spread out over a very wide temporal window, as shown in Figs. 4(a) and 4(d). Here, the blueshift of the fundamental soliton is no longer blocked by the ZDW, and the

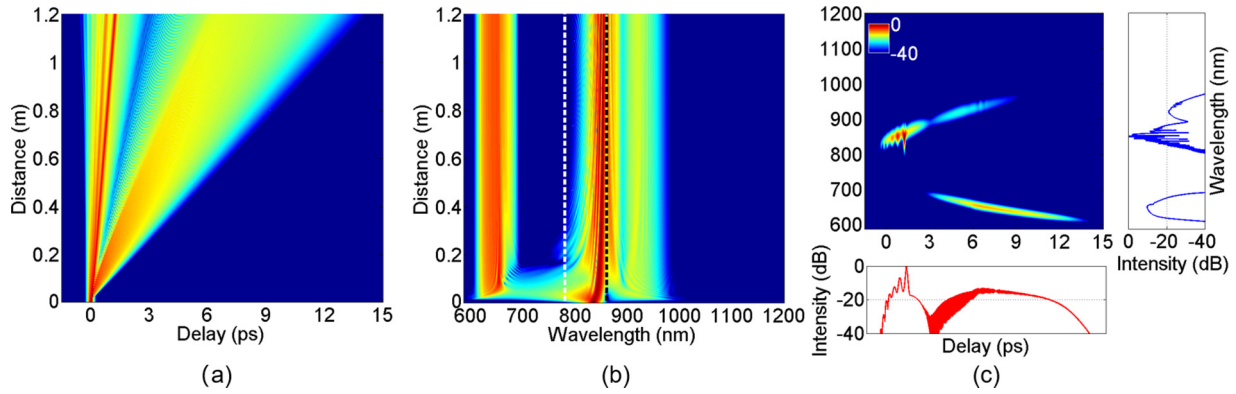


FIG. 5. (a) Temporal and (b) spectral evolutions of higher-order soliton in a 1.2-m-long PCF with one ZNW located at 860 nm for $\gamma_{\text{eff}} = 1.1357 \times 10^{-2} \text{ W}^{-1} \text{ m}^{-1} \text{ ps}$. (c) The corresponding spectrogram as well as the temporal and spectral profiles at the PCF output. The vertical white (black) dashed line in (b) marks the ZDW (ZNW) at 780 nm (860 nm).

fundamental soliton occupies the nonsoliton region where solitons are not supposed to form. Since the nonsoliton region is made very narrow by bringing the ZNW close to the ZDW, the soliton (2) can tunnel part of its energy through the spectrally limited nonsoliton region to another soliton region. Because of the SST effect, the second-ejected fundamental soliton (2) finally evolves into one soliton with a very narrow temporal width and a very broad spectrum, as shown in Fig. 4(d). The above phenomenon shows that the occurrence of the SST effect in the fibers with frequency-dependent Kerr nonlinearity requires a narrow nonsoliton region as a potential barrier sandwiched between two soliton ones. For the third fundamental soliton (labeled by 3) ejected in the vicinity of the pump wavelength, it first redshifts toward the longer wavelength under the Raman effect and then collides with the residual pump soliton pulse. The peak intensity of the soliton (3) is increased by gaining some energy from the residual pumped soliton pulse during the collision, as shown in Figs. 4(a) and 4(b). Subsequently, the soliton (3) with higher peak intensity accelerates to redshift and radiates some energy to the phase-matched DW in another soliton region, as shown in Fig. 4(d).

As the slope of the doping Kerr nonlinearity increases further from negative to positive, the ZNW will fall at a wavelength longer than the pump wavelength. In the case of $\gamma_{\text{eff}} = 1.1357 \times 10^{-2} \text{ W}^{-1} \text{ m}^{-1} \text{ ps}$, the ZNW is located at 860 nm. Thus, the region between the ZDW and ZNW is soliton while outside the region it is nonsoliton, which provides an essential prerequisite for the generation of BDW and RDW. Under the combined action of higher-order dispersion and Raman effect, the higher-order soliton pulse breaks into a series of fundamental solitons in the soliton region via soliton fission as well as the BDW and RDW in the nonsoliton region via satisfying the phase-matching condition. When the generated fundamental soliton gradually redshifts toward the longer wavelength via Raman-induced frequency shift, the spectrum of RDW blueshifts toward the ZNW with further propagation. Since the ZNW is near the pump frequency, it brings the Raman-induced frequency shift of the generated fundamental solitons to a halt quickly, as shown in Fig. 5(b). The suppression of the Raman-induced frequency shift makes the generated fundamental soliton confined in a specific

narrow spectral band close to the ZNW. In this case, more energy is transferred to the nonsoliton region, and as a result the intensities of the BDW and RDW are significantly enhanced. In the fiber with two ZDWs, the presence of the second ZDW plays a pivotal role in arresting the Raman redshift of the fundamental soliton and inducing the generation of the RDW. Most previous studies have shown that the cancellation of the Raman-induced frequency shift is due to the process of spectral recoiling associated with the emission of the RDW, which is made possible by the negative dispersion slope in the fibers with two ZDWs [7,24]. However, the same phenomenon is observed in the present work by a totally different effect where not the dispersion but the nonlinear slope restricts the Raman redshift of fundamental solitons in the PCF with frequency-dependent Kerr nonlinearity [17].

IV. CONCLUSIONS

In this work, we have studied the evolution of a higher-order soliton pulse in PCFs with one ZNW in addition to one ZDW. By regulating the magnitude of nonlinear dispersion, the strength of the effective doping nonlinearity and the position of the ZNW change dramatically, which plays a major role in manipulating the generation and distribution of the fundamental solitons and DWs during the higher-order soliton evolution. When the ZNW coincides with the ZDW at 780 nm, the blueshifted fundamental soliton that satisfies the phase-matching and group-velocity-matching conditions with the redshifted fundamental soliton is ejected during the fission of a higher-order soliton. When there is a minor interval between the ZNW at 760 nm and the ZDW, the SST phenomenon occurs in the PCF with frequency-dependent Kerr nonlinearity, namely, one soliton tunneling from one soliton region to another one through a spectrally limited nonsoliton region. When the ZNW at 860 nm is longer than the ZDW and close to the pump wavelength, the slope of the doping nonlinearity brings the Raman shift of the ejected fundamental solitons to a halt quickly and helps the generation of high-intensity BDW and RDW. Such rich phenomena of higher-order soliton evolution in the PCFs with one ZDW and one ZNW mainly results from a high flexibility in the effective doping nonlinearity.

ACKNOWLEDGMENTS

This work was supported by the National Natural Science Foundation of China (Grant No. 62105295) and Science and Technology Research Project of Henan Province (Grant No. 222102210099).

-
- [1] G. P. Agrawal, *Nonlinear Fiber Optics*, 5th ed. (Academic Press, Oxford, 2013).
- [2] J. M. Dudley, G. Genty, and S. Coen, Supercontinuum generation in photonic crystal fibers, *Rev. Mod. Phys.* **78**, 1135 (2006).
- [3] A. V. Husakou and J. Herrmann, Supercontinuum Generation of Higher-Order Soliton by Fission in Photonic Crystal Fibers, *Phys. Rev. Lett.* **87**, 203901 (2001).
- [4] P. St. J. Russell, Photonic crystal fibers, *Science* **299**, 358 (2003).
- [5] C. Markos, J. C. Travers, A. Abdolvand, B. J. Eggleton, and O. Bang, Hybrid photonic-crystal fiber, *Rev. Mod. Phys.* **89**, 045003 (2017).
- [6] K. M. Hilligsøe, T. V. Anderson, H. N. Paulsen, C. K. Nielsen, K. Mølmer, S. Keiding, R. Kristiansen, K. P. Hansen, and J. J. Larsen, Supercontinuum generation in a photonic crystal fiber with two zero dispersion wavelengths, *Opt. Express* **12**, 1045 (2004).
- [7] W. Wang, H. Yang, P. Tang, C. Zhao, and J. Gao, Soliton trapping of dispersive waves in photonic crystal fiber with two zero dispersive wavelengths, *Opt. Express* **21**, 11215 (2013).
- [8] E. N. Tsoy and C. M. de Sterke, Theoretical analysis of the self-frequency shift near zero-dispersion points: Soliton spectral tunneling, *Phys. Rev. A* **76**, 043804 (2007).
- [9] H. Guo, S. Wang, X. Zeng, and M. Bache, Understanding soliton spectral tunneling as a spectral coupling effect, *IEEE Photonics Technol. Lett.* **25**, 1928 (2013).
- [10] S. Zhao, H. Yang, Y. Zhao, and Y. Xiao, Supercontinuum manipulation based on the influence of chirp on soliton spectral tunneling, *Chin. Phys. B* **27**, 114219 (2018).
- [11] S. Wang, H. Guo, D. Fan, X. Bai, and X. Zeng, Analysis of cascaded soliton spectral tunneling effect in segmented fibers with engineered dispersion, *IEEE Photonics J.* **5**, 6100608 (2013).
- [12] A. Lin, X. Liu, P. R. Watekar, Y. Chung, and W. Han, Ag nanocrystal-incorporated germano-silicate optical fiber with high resonant nonlinearity, *Appl. Phys. Lett.* **93**, 021901 (2008).
- [13] R. Driben and J. Herrmann, Solitary pulse propagation and soliton-induced supercontinuum generation in silica glasses containing silver nanoparticles, *Opt. Lett.* **35**, 2529 (2010).
- [14] E. Verhagen, L. Kuipers, and A. Polman, Enhanced nonlinear optical effects with a tapered plasmonic waveguide, *Nano Lett.* **7**, 334 (2007).
- [15] L. Bigot, H. E. I. Hamzaoui, A. Le Rouge, G. Bouwmans, F. Chassagneux, B. Capoen, and M. Bouazaoui, Linear and nonlinear optical properties of gold nanoparticle-doped photonic crystal fiber, *Opt. Express* **19**, 19061 (2011).
- [16] R. Driben, A. Husakou, and J. Herrmann, Low-threshold supercontinuum generation in glasses doped with silver nanoparticles, *Opt. Express* **17**, 17989 (2009).
- [17] S. Bose, R. Chattopadhyay, S. Roy, and S. K. Bhadra, Study of nonlinear dynamics in silver-nanoparticle-doped photonic crystal fiber, *J. Opt. Soc. Am. B* **33**, 1014 (2016).
- [18] S. Zhao and X. Sun, Soliton dynamics in an all-normal-dispersion photonic crystal fiber with frequency-dependent Kerr nonlinearity, *Phys. Rev. A* **102**, 033514 (2020).
- [19] S. Bose, A. Sahoo, R. Chattopadhyay, S. Roy, S. K. Bhadra, and G. P. Agrawal, Implications of a zero-nonlinearity wavelength in photonic crystal fibers doped with silver nanoparticles, *Phys. Rev. A* **94**, 043835 (2016).
- [20] F. R. Arteaga-Sierra, A. Antikainen, and G. P. Agrawal, Soliton dynamics in photonic-crystal fibers with frequency-dependent Kerr nonlinearity, *Phys. Rev. A* **98**, 013830 (2018).
- [21] N. Zhavoronkov, R. Driben, B. A. Bregadiolli, M. Nalin, and B. A. Malomed, Observation of asymmetric spectrum broadening induced by silver nanoparticles in heavy-metal oxide glass, *Europhys. Lett.* **94**, 37011 (2011).
- [22] C. Liu, E. J. Rees, T. Laurila, S. Jian, and C. F. Kaminski, Periodic interactions between solitons and dispersive waves during the generation of non-coherent supercontinuum radiation, *Opt. Express* **20**, 6316 (2012).
- [23] M. H. Frosz, O. Bang, and A. Bjarklev, Soliton collision and Raman gain regime in continuous-wave pumped supercontinuum generation, *Opt. Express* **14**, 9391 (2006).
- [24] D. V. Skryabin, F. Luan, J. C. Knight, and P. S. J. Russell, Soliton self-frequency shift cancellation in photonic crystal fibers, *Science* **301**, 1705 (2003).